

Thermal stability and lifetime of [AMIM]Cl-PFSA composite membranes

Yi-heng Lu¹ · Yong Cao¹ · Yu-wei Lu² · Tao Yang¹

Received: 23 July 2016 / Accepted: 13 December 2016 / Published online: 4 January 2017
© Akadémiai Kiadó, Budapest, Hungary 2017

Abstract 1-Allyl-3-methylimidazolium chloride [AMIM]Cl hybrid perfluorosulfonic acid (PFSA) composite electrolyte membrane was prepared and characterized by TG and FTIR technique. The conductivity was measured using AC impedance method. The results showed that when raised from 20 to 90 °C, the conductivity of composite membrane was increased from 4.50×10^{-6} to 1.34×10^{-5} S cm⁻¹, before and after the modification of triethylamine, the thermal stability of composite membrane was not changed, but the TEA-PFSA with [AMIM]Cl reactivity was a little difference. However, the heat resistance of composite membrane was significantly enhanced compared with that of PFSA membrane, the peak temperature of composite membrane almost disappeared in first stage, and offset to the high-temperature zone. When heated at 350 °C, the decomposition rate of PFSA, 10%[AMIM]Cl-PFSA and 10%[AMIM]Cl-TEA-PFSA membrane was 13.71, 3.67 and 1.26%, respectively. If the decomposition process follows isothermal first-order reaction and the conversion rate α is 10%, the activation energy E_{α} of the composite membrane is 97.4 kJ mol⁻¹. Besides, the isothermal lifetime of composite membrane was also measured.

Keywords 1-Allyl-3-methylimidazolium chloride · Ionic liquids · Perfluorinated sulfonic acid · Composite membrane · Thermal stability · Lifetime

List of symbols

θ	Reaction time taken to attain a particular α at infinite temperature
a, b	The constant when reaction fraction α is certain
E (kJ mol ⁻¹)	Activation energy
E_{α} (kJ mol ⁻¹)	Activation energy when reaction fraction is α
R (J mol ⁻¹ K ⁻¹)	Gas constant
$f(\alpha)$	Differential mechanism function
$g(\alpha)$	Integral mechanism function
t (min)	Reaction time or thermal life
$t_{0.5}$ (min)	Time required to convert 50%
t_{α} (min)	Time required to convert reaction fraction α
$d\alpha/d\theta$	Generalized reaction rate
A	The pre-exponential factor of Arrhenius
α	Reaction fraction
β (K min ⁻¹)	Heating rates
pH	Potential of hydrogen
T (K)	Reaction temperature
T_0 (K)	Isothermal reaction temperature
TG (%)	Thermo-gravimetry
DTG (% min ⁻¹)	Differential thermo-gravimetry
$d\alpha/dt$ (% min ⁻¹)	Decomposition rate
Z' (Ω)	Impedance value (real part in Nyquist figure)
Z'' (Ω)	Impedance value (imaginary part in Nyquist figure)
r	Linear correlation coefficient
SD	Standard deviation
σ (S cm ⁻¹)	Proton conductivity
L (cm)	Film thickness
R (Ω)	Membrane resistance

✉ Yi-heng Lu
yhlu2000@163.com

¹ School of Chemical Engineering, Anhui University of Science and Technology, Huainai 232001, China

² Laboratoire de Chimie Physique, Université de Paris Sud, 91405 Orsay Cedex, France

S (cm ²)	Membrane area
W_1	The mass of membrane after soak
W_0	The quality of membrane before soaking
S_{wet}	Wet membrane area after dipping
S_{dry}	Dry area before immersion
H^+	Hydrogen proton
W_{wet}	The quality of membrane after the reaction
W_{dry}	Mass of membrane before the reaction

Introduction

Proton exchange membrane is a key component of polymer electrolyte membrane fuel cells. The latter is considered one of the most promising technologies for hydrogen–oxygen fuel power generation, besides they will play a leading role in all fuel cell technologies for H₂ fuel vehicles. The PEM fuel cell system is currently subject to catalyst CO poisoning and PEM operating temperature limit, mainly the membrane itself working temperature limit. The membranes currently available for PEM fuel cells are predominantly Nafion membranes, which exhibit good performance only at around 80 °C. The key issue is that the proton conductivity of the Nafion membrane is highly dependent on the presence of water in the membrane [1].

In order to solve these problems, it is necessary to develop novel PEMs which exhibit less humidity dependency and good thermal stability at elevated temperatures in which water and thermal management as well as catalytic activity are greatly improved. A common way to improve the water retention of membranes above 100 °C is by incorporating hydrophilic/hygroscopic inorganic additives such as silica [2], titanium dioxide [3] and heteropolyacids [4] into the Nafion membrane. The pore/channel structure of the host polymers such as polyhedral oligomeric silsesquioxanes (POSSs) [5], zeolites [6] and montmorillonite (MMT) [7] not only increases water uptake, but also provides additional proton transport in the membrane. In order to improve the thermal stability of the polymer backbone, the aromatic sulfuric acid moiety has been studied as an alternative to Nafion in various polymers including sulfonated poly (2,6-dimethyl-1,4-phenylene oxide) [8], Sulfonated polyimides [9], sulfonated polybenzimidazoles [10–12], sulfonated poly (sulfones) [13] and sulfonated polyether ketones [14–16] etc.

However, all of these sulfonated ionomer membranes are still susceptible to loss of conductivity when water is lost. Water is necessary for proton conductivity because it promotes proton dissociation from the hydrophilic sulfonic acid and provides a highly mobile hydrated proton. Water

also expands the membrane and allows bridging between ion inclusions that promote proton conductivity. Due to their water dependency, the operation of these sulfonated membranes is still limited to temperatures below 120 °C. For operation of PEM fuel cells with temperature greater than 150 °C, a non-aqueous proton transfer mechanism is required. Imidazole is a candidate exhibiting considerable proton conductivity in the pure state. Although phosphoric acid exhibits a very high degree of self-dissociation, such as doped polybenzimidazole (PBI) [11, 15, 17] or Nafion membrane with phosphoric acid to increase its conductivity, but at high temperatures phosphoric acid is readily dehydrated to form poly-phosphoric acid leads to a decrease in conductivity. In addition, phosphoric acid is readily soluble in water and is diluted with the resulting water, reducing its concentration.

In recent years, ionic liquids as a new class of strong polar solvents have attracted wide attention in different fields. Ionic liquids are room temperature molten salts typically comprised of bulky asymmetric organic cations and inorganic anions and have many particularly attractive properties such as non-volatile, non-combustible, high thermal stability, high ionic conductivity and wide electrochemical stability windows [18–34].

Ionic liquids are widely used as fillers in the following framework materials, for example, Ionic conducting material [35], large pore zeolites absorbed the ionic liquid, 2-hydroethyl trimethylammonium dimethyl phosphate[HETMA](CH₃)₂PO₄), *N,N*-dimethyl-*N*-(2-hydroxyethyl) ammonium bis(trifluoromethanesulfonyl) imide[DMHA]BTf and 1-methylimidazolium bis(trifluoromethanesulfonyl)imide [MIM] BTf coupled to the polybenzimidazole membrane used for high-temperature PEMFCs [6]. Low acid leaching PEM fuel cells based on polybenzimidazole nanocomposite-doped polar ionic liquid were developed [36]. Performance of new polyethylene/ionic liquids as an electrolyte for the base membrane in PEMFCs was investigated [37]. Based on sulfonated polyether ketones-doped polar ionic liquid anhydrous new composite membrane, its conductivity is 5 mS cm⁻¹ at 140 °C [38]. Ionic liquid 1-hexyl-3-methylimidazolium [BF₄] was doped with Nafion/polyethyleneoxide (PEO) composite membrane substrate for CO₂/CH₄ [39]. Design of Nafion membrane combined with different ionic liquids, the impact of Nafion on the degree of binding of cationic ions, such as the phenyltrimethylammonium chloride [TPMA]Cl, *n*-dodecyltrimethylammonium chloride [DTA]Cl, hexadecyltrimethylammonium bromide [CTA]Br, 1-*n*-butyl-3-methylimidazolium tetrafluoroborate [BMIM]BF₄ and 1-*n*-octyl-3-methylimidazolium hexafluorophosphate [OMIM]PF₆ cationic ions, was discussed [40]: study of imidazolium cation structure (1-ethyl-3-methylimidazolium tetrafluoroborate [EMIM]BF₄, 1-butyl-3-methyl tetrafluoroborate [BMIM]BF₄) on direct electrochemical and bioelectrocatalytic of Nafion group peroxidase [41].

Investigation of high-temperature proton exchange membrane based on 1-butyl-3-methylimidazolium chloride cations and phosphate doped with the Nafion membrane; a conductivity of 10.9 mS cm^{-1} was obtained [42].

In spite of the extensive efforts made in recent years for high-temperature membrane, none of the membranes so far have met all of the operating requirements of PEM fuel cells above $150 \text{ }^\circ\text{C}$. The problem of isothermal durability and thermal life of the composite electrolyte membrane for fuel cells is far from being solved and is rarely reported in the literature. Considering the fact that Nafion membranes are expensive, Nepem-112 (perfluorinated sulfonic acid ion exchange membranes, called PFSA) membrane-doped ionic liquids 1-allyl-3-methylimidazolium chloride [AMIM]Cl have not been reported as proton exchange membrane materials for fuel cells. This work is intended to demonstrate that the feasibility of the ionic liquid [AMIM]Cl interacts with PFSA or with TEA-PFSA to form a complex proton-conducting membrane and acts as the actual membrane for PEM fuel cell operation.

The thermogravimetric analysis of [AMIM] Cl-PFSA and [AMIM] Cl-TEA-PFSA composite membranes before and after the reaction showed that the peak temperature of 10% [AMIM]Cl-PFSA composite membrane in first stage of thermal degradation almost disappeared owing to the PFSA membrane heat resistant significantly enhanced, and offset to high-temperature region. When heated at $350 \text{ }^\circ\text{C}$, the conversion rate of PFSA, 10% [AMIM]Cl-PFSA and 10% [AMIM]Cl-TEA-PFSA membrane was 13.71, 3.67 and 1.26%, respectively. It can be seen that 10% [AMIM]Cl-TEA-PFSA composite membrane is stable at $350 \text{ }^\circ\text{C}$. When raised from 20 to $90 \text{ }^\circ\text{C}$, the conductivity of composite membrane was increased from 4.50×10^{-6} to $1.34 \times 10^{-5} \text{ S cm}^{-1}$.

If the decomposition process obeys isothermal first-order reaction and the conversion rate α is 10%, the activation energy E_α of the 10% [AMIM]Cl-PFSA composite membrane is 97.4 kJ mol^{-1} and the pre-exponential factor A was $2.13 \times 10^5 \text{ min}^{-1}$. According to the generalized kinetic equations and the master plots drawn from the isothermal data and the first-order reaction, the $d\alpha/d\theta/(d\alpha/d\theta)_{\alpha=0.5}$ versus α , the $\theta/\theta_{0.5}$ versus α and the $(d\alpha/d\theta)\theta$ versus α , the theoretical master curves of the 10% [AMIM]Cl-PFSA composite membranes were compared with the experimental mater plots.

Experimental

Materials and equipment

Proton exchange membrane (PFSA membrane), a colorless transparent, model Nepem-112, a thickness of $50 \text{ }\mu\text{m}$, the tensile modulus of 630 MPa , which was purchased from the

Jiangsu HuaiAn Kerun film material Co. Jiangsu, China; concentrated sulfuric acid, hydrogen peroxide, ferricyanide, ferrous potassium cyanide, potassium chloride, triethylamine (TEA) were all in reagent grade pure and without purified. 1-allyl-3-methylimidazolium chloride [AMIM]Cl (referred to ILs) ionic liquid (99 mass%) was purchased from the Shanghai Cheng jie Chemical Co. in China. The electrochemical workstation was purchased from the Shanghai Chen Hua Instrument Co. in China, model CHI660D. Conductivity meter was the model DDS-307A, produced by the Hailei magnetic limited. Digital pH meter was the model CT-6220 produced by the Shenzhen Ke Dida Electronics Co. in China. ATR-FTIR spectroscopic meter, Nicolet 8700, Thermo Scientific Instrument Co. U.S.A.

Configuration of the electrolyte solution: Weigh 5 mmol of $\text{K}_3\text{Fe}(\text{CN})_6$ and 5 mmol of $\text{K}_4\text{Fe}(\text{CN})_6 \cdot \text{H}_2\text{O}$ and 0.1 mol of KCl formulated into 1 L aqueous solution.

Preparation of ionic liquids/PFSA composite membrane

Pretreatment of membranes

A size of $1.0 \times 2.0 \text{ cm}$ PFSA membrane was cleaned with deionized water at room temperature for 24 h, then allowed to stand at $80 \text{ }^\circ\text{C}$ for 1 h with 1 mass% H_2O_2 solution, placed in deionized water at $80 \text{ }^\circ\text{C}$ impregnating 1 h, put out, then put into 0.5 M sulfuric acid solution and boiled at $80 \text{ }^\circ\text{C}$ for 1 h, brought out, washed with deionized water to neutral, and vacuum dried at $80 \text{ }^\circ\text{C}$ for 8 h, and the PFSA- H^+ membranes were obtained.

Preparation of TEA/PFSA membrane

PFSA- H^+ was immersed in the 1 mol L^{-1} TEA ethanol water (1:1 mass) solution, stirred for 12 h, washed with deionized water, removed, and dried in vacuum 8 h, and TEA/PFSA membrane was obtained.

Preparation of composite membrane

5, 10 and 20 mass% [AMIM]Cl aq. solution was prepared; then, the PFSA- H^+ and TEA-PFSA membranes were immersed, respectively, in it at $30 \text{ }^\circ\text{C}$ for 48 h, removed, placed in $80 \text{ }^\circ\text{C}$ vacuum dried for 8 h, weighed to give [AMIM]Cl-PFSA and [AMIM]Cl-TEA-PFSA composite membrane.

TG

Thermal analysis were recorded on the Shimadzu, model DTG-60H, a heating rate of $10 \text{ }^\circ\text{C min}^{-1}$, a platinum crucible was used as reference for non-isothermal

measurement, the carrier gas was nitrogen gas, the temperature was at the range of 25–700 °C, flow rate of 75 mL min⁻¹, and the quality of the sample was 3.50–4.50 mg.

Impedance conductivity

CHI660D electrochemical workstation, impedance frequency range of 1.0–1.0 × 10⁶ Hz, the disturbance voltage was 10 mV. Tested with a three-electrode electrochemical impedance analyzer system, the reference electrode was a saturated calomel electrode, an auxiliary electrode was Ag–AgCl electrode, and a platinum working electrode was a carbon electrode.

Water absorption

Take a size of 1.0 × 2.0 cm of 5, 10 and 20%[AMIM]Cl-PFSA composite membrane, and when placed in 80 °C dried 8 h, cooled to room temperature, and taken out, the quality scales. The membrane was placed in deionized water at 25 °C for 24 h, till the water-absorbing process is completed, the membrane quality after weighing; the different absorption coefficient of water absorption is calculated according to formula (1):

$$\text{Water absorption} = (W_1 - W_0)/W_0 \times 100\% \quad (1)$$

W_1 is the mass of membrane after soak; W_0 is the quality of membrane before soaking.

Swelling ratio

Take a 5, 10 and 20%[AMIM]Cl-PFSA composite membrane of 1.0 × 2.0 cm size, rinsed with deionized water, the membrane was placed 80 °C for complete drying 8 h, cooled to room temperature, and taken out, measuring the size of the membrane. The membrane is placed in deionized water at 25 °C for 24 h, measuring the dimensions of the membrane is completed, and the swelling ratio is calculated according to formula (2):

$$\text{Swelling ratio} = (S_{\text{wet}} - S_{\text{dry}})/S_{\text{dry}} \times 100\% \quad (2)$$

S_{wet} is wet membrane area after dipping, S_{dry} is dry area before immersion.

Results and discussion

[AMIM]Cl aqueous solution pH and conductivity

Table 1 shows pH and conductivity of ionic liquids aqueous solution before and after immersion of PFSA membrane. From the table, the pH of the reaction solution decreases with increasing concentration of ionic liquids

solution, this is because when the PFSA was immersed in an aqueous solution of ionic liquids, its H⁺ proton in PFSA is replaced by the imidazole cations, resulting in enhancement of the acid concentration of the solution. The conductivity increases with the concentration of ionic liquids; this is due to the increase of the cations and anions of ionic liquids. After reaction, the conductivity indicated a little decrease is because a weak electrolyte is generated between the perfluorooctane sulfonate anion and the imidazole cation, resulting in conductivity of a solution was reduced.

Mass gain

The weight gain of composite membrane is calculated according to formula (3):

$$\text{Weight gain} = (W_{\text{wet}} - W_{\text{dry}})/W_{\text{dry}} \times 100\% \quad (3)$$

where W_{wet} is the quality of membrane after the reaction, W_{dry} is mass of membrane before the reaction. After immersed for 48 h, the concentration of [AMIM]Cl is 5, 10 and 20 mass%, the rate of weight gain of [AMIM]Cl-PFSA composite membrane is 12.89, 9.88 and 10.48%, respectively. It shows that the quality of composite membrane after the reaction increased, suggesting that some of [AMIM]Cl penetrated into the pores of the PFSA membrane.

Water absorption

The [AMIM]Cl-PFSA composite membrane formed from different concentrations of ionic liquids was placed in deionized water, maintained at 80 °C for 24 h. After completion of the reaction, the membrane was removed, measured and recorded. Compared the quality of membrane to immersion before, Fig. 1 shows the water absorption of membranes. It can be seen from a bar graph that the water absorption of [AMIM]Cl-composite membrane was increased. With increasing concentration of ionic liquid, water absorption of composite membrane is also increased and water absorption for 20%[AMIM]Cl-PFSA is nearly 10 times than that of PFSA membrane.

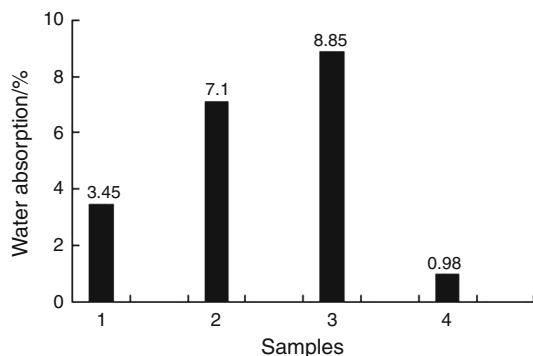
Swelling ratio

Measuring the size of the dry state membrane, the membrane was placed in deionized water and heated swell for 24 h, and then wet membrane was measured. According to rate of the swelling, the swelling ratio contrast histogram is plotted in Fig. 2. As shown in figure, PFSA membrane has the highest swelling ratio of 13.1. The swelling ratios of composite membrane are less than that of PFSA, with the increasing concentration; the swelling ratio is decreasing.

Table 1 pH and conductivity σ of [AMIM]Cl aqueous solution before and after immersion of PFSA membrane

No.	Dipping time/h	Concentration/mass%	Before reaction		After reaction	
			pH	$\sigma/\text{mS cm}^{-1}$	pH	$\sigma/\text{mS cm}^{-1}$
1	48	5	7.17	17.1	3.69	16.9
2	48	10	6.82	25.8	3.50	24.3
3	48	20	6.51	36.1	3.27	31.9
4	48	10	7.23	24.3	7.12	24.5

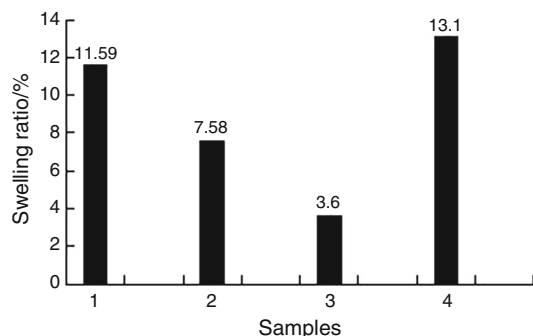
Media is water, dipping temperature: 25 °C, No. 4 denotes 10%[AMIM]Cl-TEA-PFSA membrane, No. 1, 2, 3 denotes 5, 10 and 20%[AMIM]Cl-PFSA composite membrane respectively

**Fig. 1** Water absorption of different samples 1–5%[AMIM]Cl-PFSA; 2–10%[AMIM]Cl-PFSA; 3–20%[AMIM]Cl-PFSA; 4-PFSA

The swelling rate of 20%[AMIM]Cl-PFSA is only 3.6, less than 1/3 of PFSA. The swelling ratio of the ionic liquid doped with [AMIM]Cl-PFSA composite membranes was reduced; the swelling ratio of PFSA is increased.

IR spectra of different samples

Figure 3 shows IR spectra of different samples. Figure 3a shows IR spectrum of ILs with KBr tablet, the characteristic stretching vibration near 3148 cm^{-1} corresponding to the imidazole ring CH, 3090 cm^{-1} was due to the imidazole ring double-bond hydrogen C=CH, and the peak of

**Fig. 2** The swelling rate of different samples 1–5%[AMIM]Cl-PFSA; 2–10%[AMIM]Cl-PFSA; 3–20%[AMIM]Cl-PFSA; 4-PFSA

1647 cm^{-1} is attributed to allyl groups C=C, the peak of 1332 cm^{-1} corresponding to C≡N stretching vibration.

The characteristic peaks of the imidazolium cation (C=N) appear at 1570 cm^{-1} . Bending vibration characteristic peaks around 1449 cm^{-1} corresponding to the side chain $-\text{CH}_2\text{CH}$ vibration peak, a peak of 1170 cm^{-1} was the imidazole ring CH bending vibrations in the plane; 1000 and 951 cm^{-1} is owing to $-\text{CH}=\text{CH}$, $-\text{H}$ out of plane bond rocking bending vibration, the absorption band of the two terminal vinyl characteristic frequency, and a peak of 760 cm^{-1} is attributed to the bending vibration of outer surface of the imidazole ring CH. Near 3428 cm^{-1} has a strong absorption peak, because of the [AMIM]Cl absorbing moisture easily through hydrogen bonds with water molecules on the outer surface of the imidazole ring CH bending vibration. Probably due to the small molecular weight hydrophilic groups OH^- , when combined with the weak cation, it can only produce the ionic force within the molecules of ILs. The thermal stability of ILs depends mainly on hydrogen bonding force between the heteroatoms and between carbon and heteroatom. Therefore, thermal stability was related to the ILs cation and anion structure and properties. Both thermal stability of imidazolium cation and anion to some extent can determine the thermal stability of the ionic liquid.

Figure 3b shows the ATR-FTIR spectrum of PFSA membrane, wherein 1210 and 1150 cm^{-1} of the two peaks were the $-\text{vCF}_2-$ symmetric and asymmetric stretching peaks, around 1050 cm^{-1} is the $-\text{vSO}_3-$ symmetric stretching peak, and near 982 cm^{-1} is for the $-\text{vCF}_2-$ stretching vibration peak.

Figure 3c shows the ATR-FTIR spectrum of 20%[AMIM]Cl-PFSA composite membrane. Position of 1640 cm^{-1} is the stretching peak of allyl $\text{vC}=\text{C}$; 1570 cm^{-1} peak is characteristic peak of imidazolium cation, 1450 cm^{-1} corresponds to the side chain $-\text{vCH}_2$ and vCH bending vibration, 751 cm^{-1} is the imidazole ring, the outer surface of the vCH bending vibration, 1150 and 1220 cm^{-1} of the two peaks were $-\text{vCF}_2-$ symmetric and asymmetric stretching peak, 1050 cm^{-1} is for the

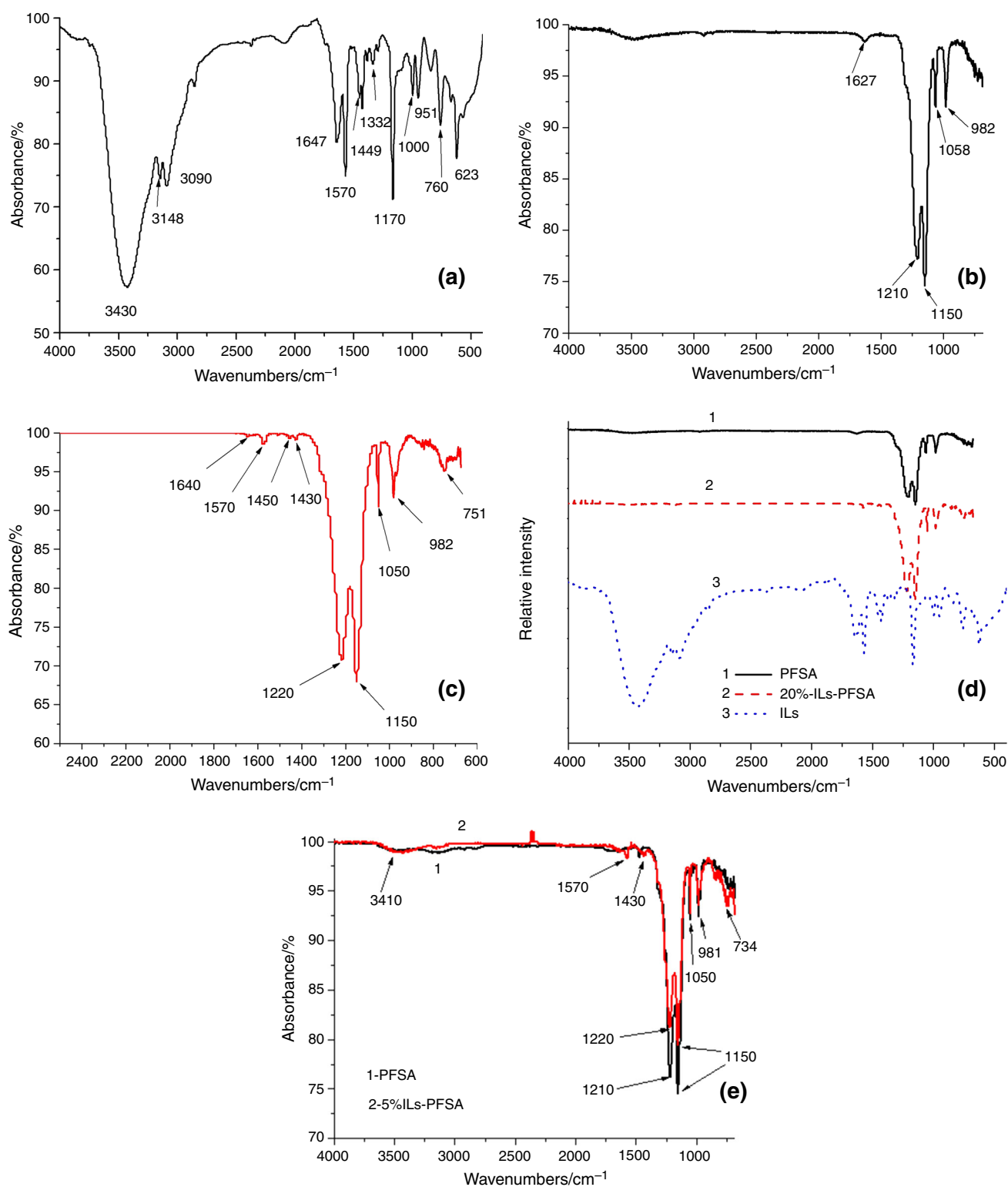


Fig. 3 IR spectra of different samples **a** [AMIM]Cl; **b** PFSA; **c** 20%[AMIM]Cl-PFSA; **d** different samples; **e** 5%[AMIM]Cl-PFSA

$-\nu\text{SO}_3-$ symmetric stretching peak, and 982 cm^{-1} is ascribed to $-\nu\text{CF}-$ stretching peaks.

Figure 3d shows FTIR spectra that compared the 20%[AMIM]Cl-PFSA with the PFSA and ILs. Infrared

analysis indicates that the structures of PFSA and composite membrane are substantially unchanged. Compared to PFSA, the composite membrane of an unknown peak at 1627 cm^{-1} disappeared. At the same time, it increased the

$\nu\text{C}=\text{C}$ vibration peaks 1640 and 1570 cm^{-1} imidazole ring of the $\nu\text{C}=\text{N}$ peaks out of the plane of the side chain $-\nu\text{CH}_2$ 1450 cm^{-1} in νCH bond swing bending vibration peak, 751 cm^{-1} νCH outer surface of the imidazole ring bending vibration peak. These additional peaks can be found in the ionic liquid, and it showed that the composite membrane may contain an ionic liquid. The reason may be due to the electrostatic attraction of the sulfonic acid groups ($-\text{vSO}_3^-$) anions of the PFSA membrane to imidazolium cations, and the formation of the van der Waals force between the interactions.

Figure 3e shows the ATR-FTIR spectra of PFSA and 5%[AMIM]Cl-PFSA composite membranes and 5%[AMIM]Cl-PFSA composite membranes was compared with PFSA membrane, resulting in a new peak vibration: 3410 cm^{-1} is NH stretching vibration, 1570 cm^{-1} peak vibration is due to characteristic peaks of cationic imidazole ring; 1430 cm^{-1} peak vibration is owing to the bending vibration of $\text{CH}=\text{CH}_2$; 734 cm^{-1} ascribed to NH degeneration vibration. Table 2 shows the infrared characteristic peaks of ILs, PFSA and 5%[AMIM]Cl-PFSA composite membranes, and the vibration peak emerging characteristic vibration is 1-allyl-3-methylimidazolium chloride ionic liquids peak, indicating that between [AMIM]Cl and PFSA membrane, a chemical reaction occurs. For the characteristic vibration of both peaks for $\nu-\text{CF}_2-$, $\nu-\text{SO}_3$ and $\nu\text{C}-\text{O}-\text{C}$, the peaks essentially were not changed, but the intensity of the vibration peaks decreased, while the most significant decline is 1210 cm^{-1} ascribed to $\nu-\text{CF}_2-$ group symmetric stretching vibration peak, down 21.0%, followed by the antisymmetric 1150 cm^{-1} at $-\text{CF}_2-$ group stretching vibration; the peak intensity decreased 19.5%. Thus, [AMIM]Cl doping produced a greater impact on the $-\text{CF}_2-$ group of the modified PFSA composite membrane.

Thermal stability

Figure 4 shows TG-DTG curves of composite membranes. TG curves of PFSA, 10%[AMIM]Cl-TEA-PFSA and 10%[AMIM]Cl-PFSA composite membrane of thermal degradation are shown in Fig. 4a. As shown from the figure, after the protection of triethylamine, the TG curves for 10%[AMIM]Cl-TEA-PFSA composite membrane are nearly unchanged compared to non-protection of triethylamine, which the thermogravimetric curves slightly deviated to the right, but the difference is small. After the reaction, the TG curve of 10%[AMIM]Cl-PFSA composite membrane shifted significantly to the high-temperature zone compared to the unreacted of PFSA membrane. When conversion rate is 1.5%, decomposition temperature of triethylamine pretreated and the PFSA film distributed at 356.7 and 322.7 $^{\circ}\text{C}$, that is, after triethylamine protection and the role of doping [AMIM]Cl, the resistant temperature of membrane increases to 34 $^{\circ}\text{C}$. When conversion rate reached 3.5%, representing an increase in [AMIM]Cl-TEA-PFSA 2%, decomposition temperature was 343.2 $^{\circ}\text{C}$ compared to PFSA temperature which increases to 20 $^{\circ}\text{C}$, compared with 10%[AMIM]Cl-TEA-PFSA membrane resistance low temperature 10 $^{\circ}\text{C}$. Figure 4b shows DTG curves of PFSA, 10%[AMIM]Cl-TEA-PFSA and 10%[AMIM]Cl-PFSA composite film, and the PFSA membrane undergoes significant degradation stage. After doping of ionic liquids in 300–370 $^{\circ}\text{C}$, the pyrolysis (to break a sulfonic acid group) peak temperature for 10%[AMIM]Cl-PFSA in first stage almost disappeared and shift to the high-temperature zone (350–422 $^{\circ}\text{C}$), which indicates that in this interval 10%[AMIM]Cl-PFSA composite membranes are no longer decomposition and decomposition rate decreased significantly. Comparison of triethylamine protection with the non-protection, the

Table 2 Conversion rate α of the membranes in different temperature

$T/^{\circ}\text{C}$	PFSA			10%[AMIM]Cl-PFSA			10%[AMIM]Cl-TEA-PFSA		
	α	Mass/%	$d\alpha/dt$	α	Mass/%	$d\alpha/dt$	α	Mass/%	$d\alpha/dt$
100	0.75	99.25	0	0.15	99.85	0	0.44	99.56	0
150	0.75	99.25	0	0.10	99.90	0	0.10	99.90	0
180	0.84	99.16	0	0.08	99.92	0	0.09	99.91	0
250	0.92	99.08	0.02	1.86	98.14	0.72	0.32	99.68	0.3
300	1.01	98.99	0.07	3.07	96.93	0	1.01	98.99	0
350	13.71	86.29	9.12	3.67	96.33	0.25	1.26	98.74	0.25
400	38.01	61.99	9.02	20.83	79.16	6.15	18.35	81.65	6.16
450	78.79	21.21	3.44	48.92	51.08	6.54	47.63	52.37	6.13

Mass—residual mass/%; α —conversion rate/%; $d\alpha/dt$ —decomposition rate/% min^{-1}

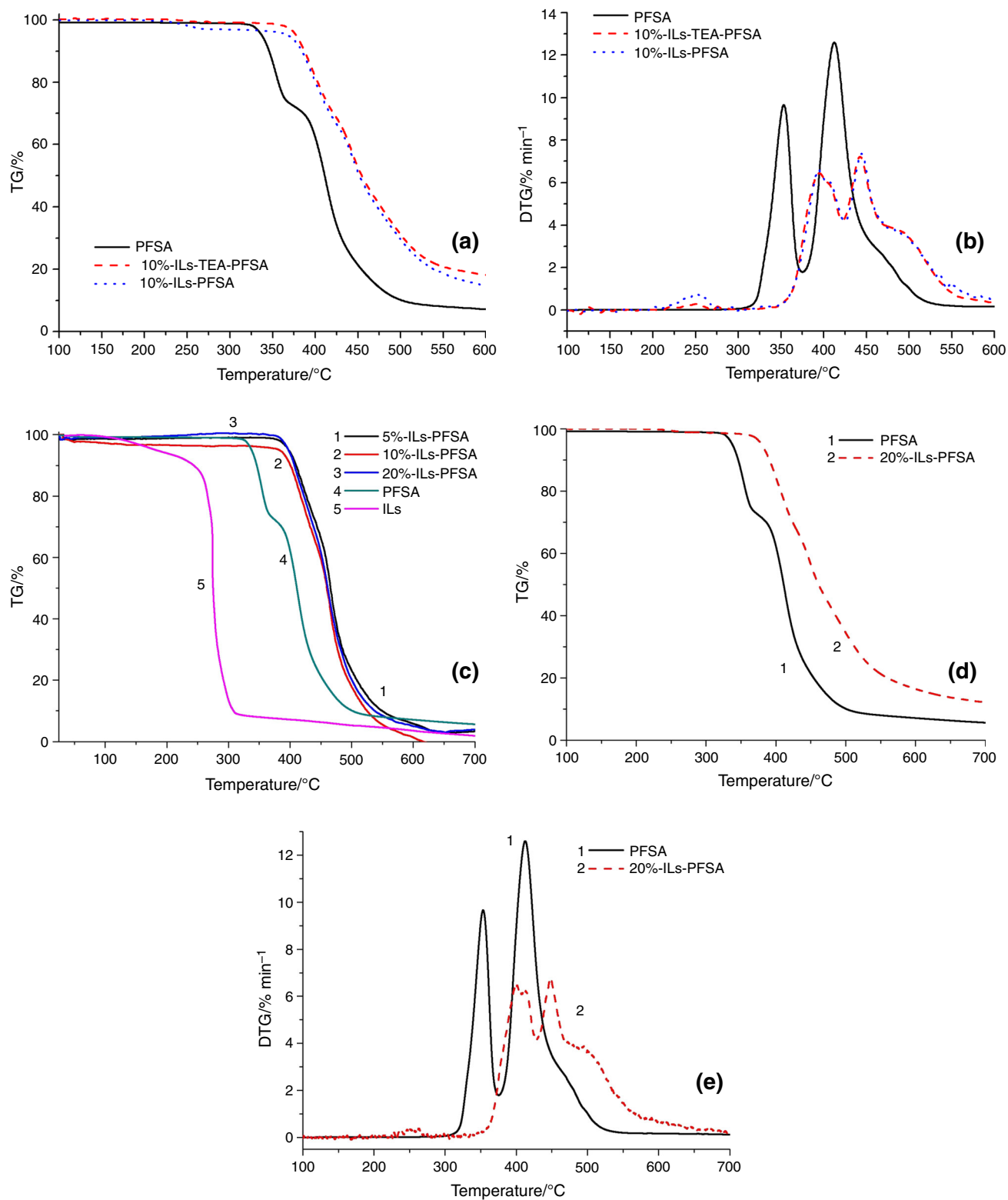


Fig. 4 TG-DTG curves of composite membranes **a** TG curves; **b** DTG curves; $\beta = 10 \text{ }^\circ\text{C min}^{-1}$; **c** [AMIM]Cl, PFSA, 5, 10, 20%[AMIM]Cl-PFSA; **d, e** TG-DTG curves of PFSA, 20%[AMIM]Cl-PFSA

differential thermogravimetric curves are substantially overlapped with no visible change in the thermal stability of the film in 370–450 °C. PFSA subjected to a second

phase of the primary side chain of thermal degradation, the peak temperature shifted to 422–474 °C, the decomposition rate drops significantly. In the range of 474–526 °C,

10% ILs/PFSA membrane generates a peak obvious pyrolysis temperature, suggesting that carbides dominated the side chain decomposition.

Figure 4c shows the TG curves of different samples, and when the conversion rate is 5%, the decomposition temperature of [AMIM]Cl, PFSA, 5%[AMIM]Cl-PFSA, 10%[AMIM]Cl-PFSA and 20%[AMIM]Cl-PFSA were 182.2, 337.5, 397.4, 382.7 and 397.4 °C. When the conversion rate reached 10%, the decomposition temperatures of [AMIM]Cl, PFSA, 5%[AMIM]Cl-PFSA, 10%[AMIM]Cl-PFSA and 20%[AMIM]Cl-PFSA were 243.6, 345.9, 409.7, 400.6 and 406.9 °C, respectively. When the conversion rate was 30%, the decomposition temperatures were 273.4, 386.1, 443.8, 432.5 and 438.2 °C. When the decomposition rate is 90%, correspondingly, the decomposition temperatures were 537.5 °C, 308.3, 501.3, 549.7 and 524.9, respectively. At 170 °C, the decomposition rate of [AMIM]Cl is less than 5%. As the temperature rises, TG curve downs sharply and when the temperature reaches 300 °C, the decomposition rate is 90%. Therefore, ionic liquid at 170 °C was stable; when it surpasses 170 °C, it will quickly decompose. As shown in figure, the results showed that when the temperature is below 320 °C, TG curves of the PFSA and the composite film are almost the same, indicating existing similar thermal stability.

TG-DTG curves of PFSA and 20%[AMIM]Cl-PFSA are shown in Fig. 4d, e. As shown in figure, TG curve of PFSA membrane and its pyrolysis experienced significant weight loss in two phases, the first stage happened in the range of 300–375 °C, its decomposition may correspond to the group of $-\text{SO}_3-$, the second stage happened when exceeded 375 °C, its peak temperature corresponding to weight loss of PFSA membrane is the main side chain decomposition. Despite of ionic liquids begins to decompose at 170 °C, but when [AMIM]Cl-PFSA composite membrane was heated, its decomposition temperature is approximately 400 °C, thermal decomposition temperature was higher than 60 °C compared to PFSA. The thermal decomposition temperature of 20%[AMIM]Cl-PFSA composite membrane significantly increased, indicating that between the ionic liquid and the PFSA membrane, there is a strong interaction formed from the electrostatic forces or Van der Waals forces, so that the thermal stability of composite membrane is increased but also indirectly verified the imidazole cationic groups that participate bonded to the anionic groups on the PFSA membrane skeleton. However, in theory with the ionic liquid concentration increasing, corresponding to the decomposition rate of the same composite membrane formed, a thermal decomposition temperature should be gradually increased. But in this TG curve this trend does not exhibit.

Figure 4d made visible, when maximum rate of decomposition for PFSA and 20%[AMIM]Cl-PFSA

composite membranes reached, the corresponding temperature was 413.1 and 448.5 °C. When higher than 310 °C, the decomposition rate of [AMIM]Cl-PFSA composite membranes was significantly higher than PFSA. Between 370 and 395 °C decomposition rate is convergence, at the range of 395–438 °C, decomposition rate of composite membrane is much higher than the PFSA. Also composite membrane thermal degradation peak 300–380 °C range goes away, the thermal decomposition behavior of composite membranes $-\text{SO}_3-$ group disappeared, and the composite film is only one stage of thermal degradation. Thus, the thermal stability of [AMIM]Cl-PFSA composite membranes was significantly better than the original film, presumably due to the ionic liquid cationic group in combination with PFSA sulfonate anion to form a stable structure and improve its thermal stability.

Table 2 shows the conversion rate (α) of the membranes in different temperature. When heated from 100 to 300 °C, the conversion rate α of PFSA membrane changed in the range of 0.75–1.01%; however, when the temperature was raised to 350–450 °C, the α of PFSA membrane rose to 13.71–78.79%, which was significantly increased. Corresponding to the decomposition rate, $d\alpha/dT$ is 9.12–3.44 (% min^{-1}).

When heated at 100–300 °C, the conversion rate α of 10%[AMIM]Cl-PFSA membrane changes in the range of 0.15–1.86%, when the temperature was raised to 350–450 °C, the α of the membrane rose from 3.67 to 48.92%. At this time, α was significantly increased. Correspondingly, the $d\alpha/dT$ obtained is 0.25–6.54 (% min^{-1}).

Equally when heated from 100 to 300 °C, α of 10%[AMIM]Cl-TEA-PFSA membranes was 0.44–1.01%, when the temperature was raised to 350–450 °C, the α of the film rose to 1.26–47.63%, at this time, α was significantly increased. Correspondingly, the $d\alpha/dT$ obtained is 0.25–6.13 (% min^{-1}).

Table 3 shows the decomposition temperature in different conversion rate. As shown from the table, when the conversion rate of PFSA, 10%[AMIM]Cl-PFSA and 10%[AMIM]Cl-TEA-PFSA film was 1 and 10%, respectively, the corresponding decomposition temperature increases from 235.0, 238.9 and 339.8 °C to 346.0, 384.4 and 387.4 °C. With increasing conversion rate, the decomposition temperature of the membrane rose.

Effect of temperature on the impedance spectroscopy

Figure 5a shows PFSA impedance spectroscopy, and at 30 °C the impedance value Z' of PFSA is 2247 Ω , and in 30–50 °C, Z' is 2250–1100 Ω ; the temperature has the greater impact on the resistance value of the film. When heated to 60–90 °C, Z' is 900–400 Ω .

Table 3 Decomposition temperature in different conversion rate

Conversion rate $\alpha/\%$	Temperature/ $^{\circ}\text{C}$		
	PFSA	10%[AMIM]Cl-PFSA	10%[AMIM]Cl-TEA-PFSA
1.0	235.0	238.9	339.8
5.0	337.5	386.6	377.7
10.0	346.0	384.4	387.4
20.0	356.7	400.0	402.8
30.0	386.1	417.3	421.6

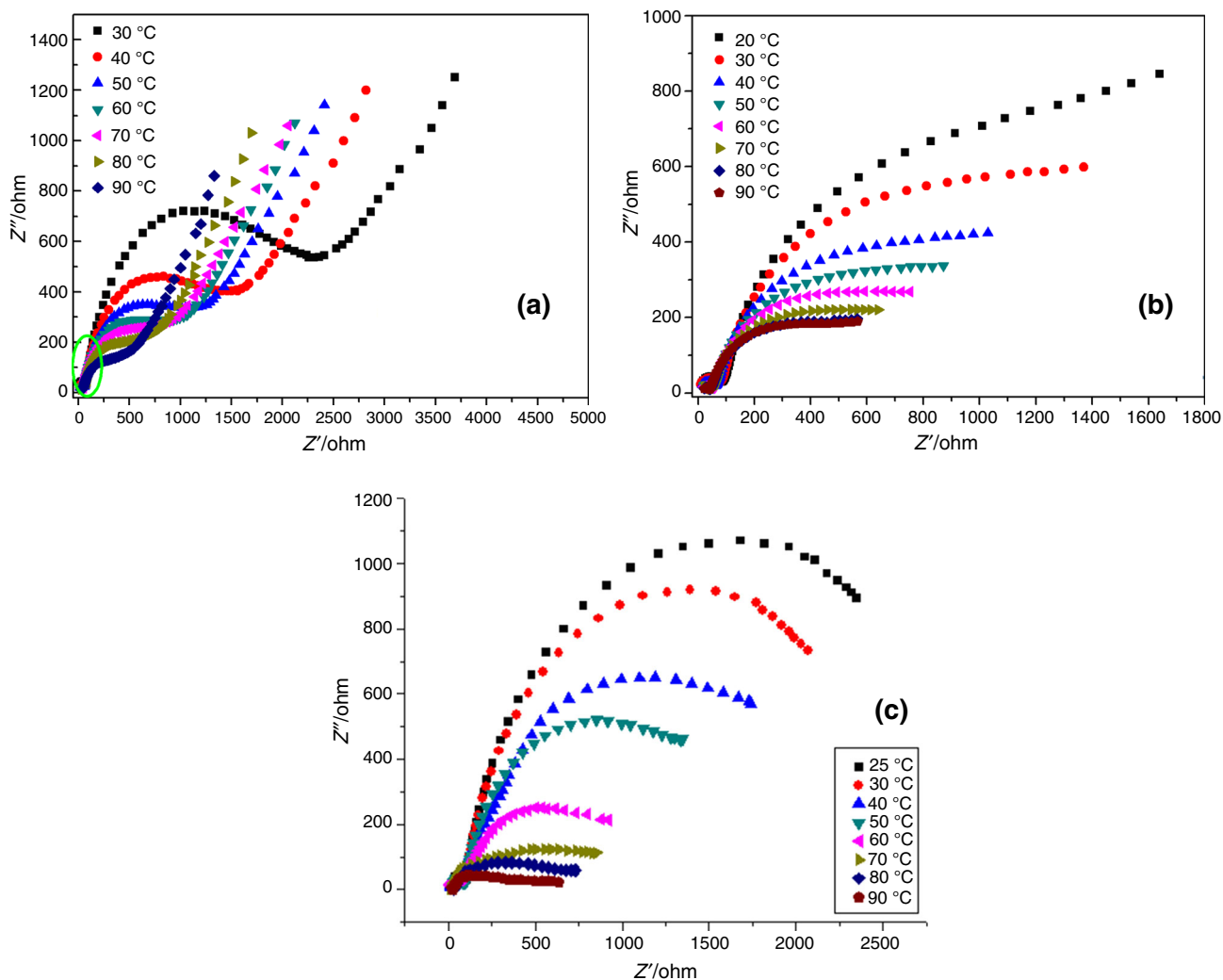
**Fig. 5** Impedance spectroscopy of composite membrane in different temperature **a** PFSA; **b** 10%[AMIM]Cl-PFSA; **c** 5%[AMIM]Cl-PFSA

Figure 5b shows impedance spectroscopy of 10%[AMIM]Cl-PFSA composite membrane. At 20 $^{\circ}\text{C}$, Z' is 1561 Ω , at 30 $^{\circ}\text{C}$, Z' is 1299 Ω , approximately 1/2 of PFSA membrane. When heated from 40 to 90 $^{\circ}\text{C}$, Z' is 1000–500 Ω , the resistance value of composite film is gradually decreased slowly. Figure 5c shows impedance

spectra of 5%[AMIM]Cl-PFSA composite membrane, at 25 $^{\circ}\text{C}$ the impedance value of composite membrane is 2652 Ω , at 30–50 $^{\circ}\text{C}$, Z' was 2272–1270 Ω , when heated to 60–90 $^{\circ}\text{C}$, Z' is 974–610 Ω , at the time, the temperature has little effect on the impedance value of composite membrane. With respect to the PFSA, the resistance of

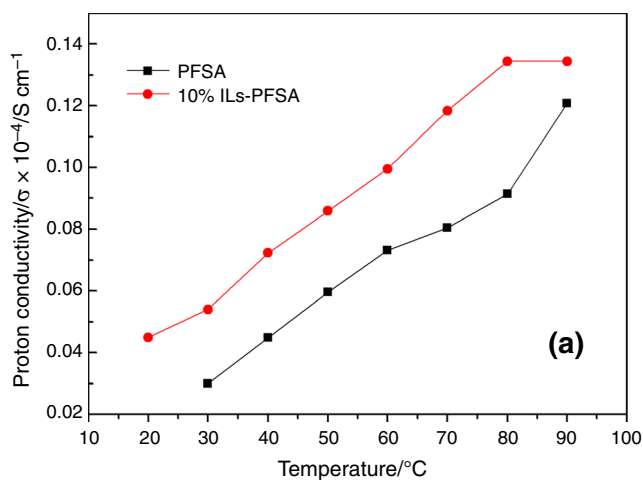
5%[AMIM]Cl-PFSA composite membrane decreased obviously.

Effect of temperature on the electrical conductivity

The proton conductivity of [AMIM]Cl-PFSA composite membrane was obtained according to formula (4):

$$\sigma = L/RS \quad (4)$$

where σ is the conductivity (S cm^{-1}), L is the distance between the two electrodes, the film thickness (cm), R is the membrane resistance (Ω), S is the membrane area (cm^2). Figure 6 shows conductivity of composite membranes. As shown in Fig. 6a, when the temperature raised from 20 to 90 °C, the conductivity of 10%[AMIM]Cl-PFSA composite membrane increased from 4.50×10^{-6} to $1.34 \times 10^{-5} \text{ S cm}^{-1}$, the conductivity of composite membrane is about 2 times than that of PFSA membrane, wherein Fig. 6b shows the conductivity of the film with temperature, when the temperature was gradually raised from 30 to 90 °C, the conductivity of PFSA membrane increases from 2.99×10^{-6} to $12.07 \times 10^{-6} \text{ S cm}^{-1}$. Correspondingly, the conductivity of 5%[AMIM]Cl-PFSA composite membrane increases from 3.30×10^{-6} to $14.35 \times 10^{-6} \text{ S cm}^{-1}$. The conductivity of composite membrane is greater than that of PFSA, and this may be due to the ionic liquid itself is an organic salt of high conductivity, proton in composite membrane more easily pass through the membrane to reach the cathode, thus improving the electrical conductivity of composite membrane.



Isothermal lifetime

The isothermal thermal decomposition data of 10%[AMIM]-PFSA composite membranes are shown in Fig. 7.

Figure 7a demonstrates the conversion rate of composite membrane changed with reaction time in 410, 415 and 425 °C, which shows the isothermal curves of weight versus t_α . Figure 7b shows the curves of $\lg t_\alpha$ versus T^{-1} ; the reacted fraction α of composite membrane was 10 and 15%, respectively. As seen from figure, two lines formed linear relationship better. TG curves were measured at 683.15, 688.15 and 693.15 K in a constant temperature (T_0), mass loss of 10 and 15% corresponding to the time t_α required, and the experimental data are shown in Table 4.

In the case of one-step decomposition process of the composite membrane under isothermal conditions (constant temperature, T_0), the time to reach a given degree of conversion can be determined by the following equation [43].

$$t_\alpha = \frac{g(\alpha)}{A \exp\left(-\frac{E_\alpha}{RT_0}\right)} \quad (5)$$

where t_α is the time/min required for the conversion rate of α , T_0 is the isothermal absolute temperature/K, R is the gas constant/ $\text{J mol}^{-1} \text{ K}^{-1}$, A is the pre-exponential factor/ min^{-1} , E_α is the activation energy/ kJ mol^{-1} , and $g(a)$ is the integral mechanism function. Equation (5) can be used to predict the lifetime of material under isothermal conditions at the temperature T_0 . Assuming that the decomposition process obeys first-order kinetics:

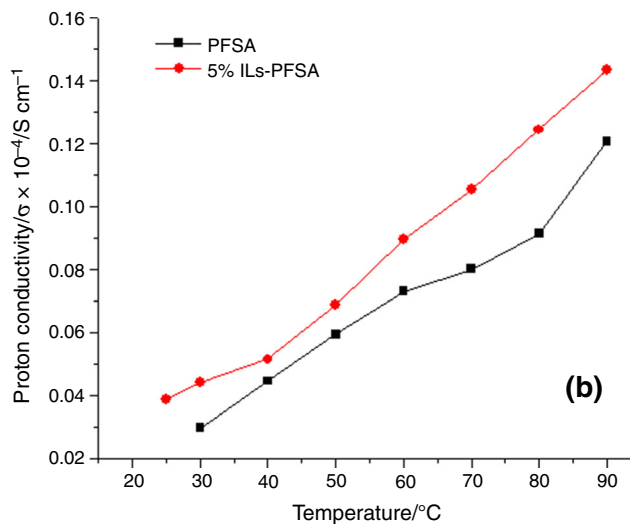


Fig. 6 Conductivity of composite membranes, a 10%[AMIM]Cl-PFSA; b 5%[AMIM]Cl-PFSA

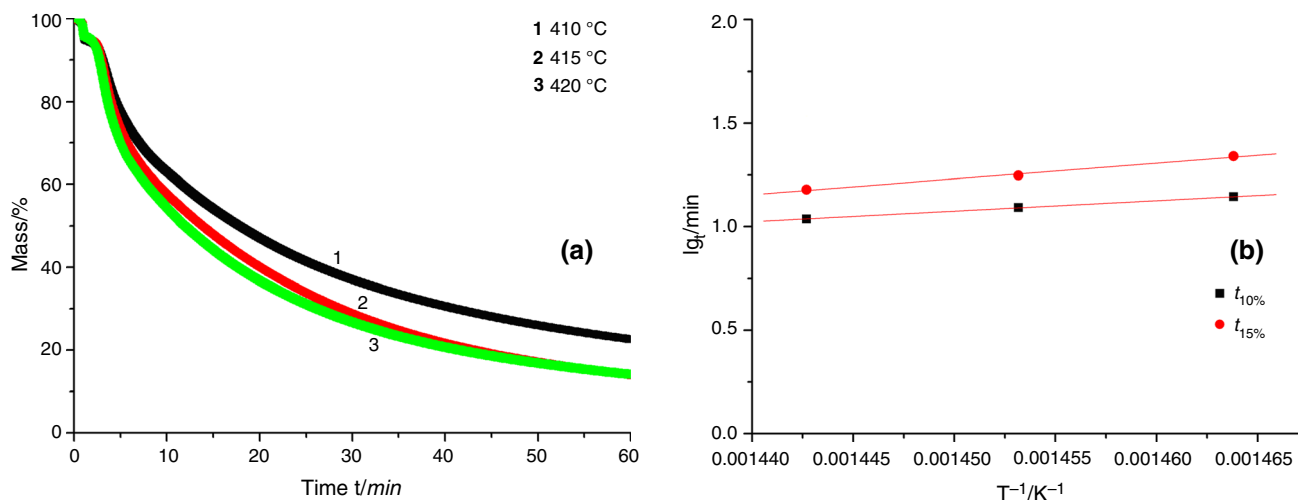


Fig. 7 Curves of isothermal mass loss of 10%[AMIM]Cl-PFSA composite membranes **a** isothermal curves of mass versus t_{α} ; **b** curves of $\lg t_{\alpha}$ versus T^{-1} when conversion rate α was 10 and 15%, respectively

Table 4 Lifetime of composite membrane in different temperature

T/K	$t_{10\%}/\text{min}$	$t_{15\%}/\text{min}$
683.15	3.14	3.82
688.15	2.98	3.48
693.15	2.82	3.25

10%[AMIM]Cl-PFSA membrane; $t_{10\%}$ and $t_{15\%}$ were the Time/min with mass loss of 10 and 15%

$$g(\alpha) = -\ln(1 - \alpha) \tag{6}$$

Substituted $g(\alpha)$ into Eqs. (5) and (6) yields the following Eq. (7):

$$t_{\alpha} = \frac{-\ln(1 - \alpha)}{A \exp\left(-\frac{E_{\alpha}}{RT_0}\right)} \tag{7}$$

On both sides of the logarithm, the following formula (8) is obtained:

$$\ln t_{\alpha} = \ln[-\ln(1 - \alpha)] - \ln A + \frac{E_{\alpha}}{RT_0} \tag{8}$$

When α certain, E_{α} and A are constant, take conversion rate α of 10%, plot $\ln t_{\alpha}$ and T_0^{-1} straight line, if a linear relationship formed, then the A and E_a can be calculated by the slope and the intercept and according to Table 4, then the slope is 5.089×10^3 and the intercept is -6.305 , where linear coefficient r is 0.9998, SD is 0.00966, then $E_{\alpha} = 97.4 \text{ kJ mol}^{-1}$, $A = 2.13 \times 10^5 \text{ min}^{-1}$. If the constant temperature operation at $T_0 = 150 \text{ }^{\circ}\text{C}$, $\alpha = 10\%$, according to Eq. (7), the thermal life $t_{10\%}$ of the composite membrane is $8.83 \times 10^3 \text{ h}$.

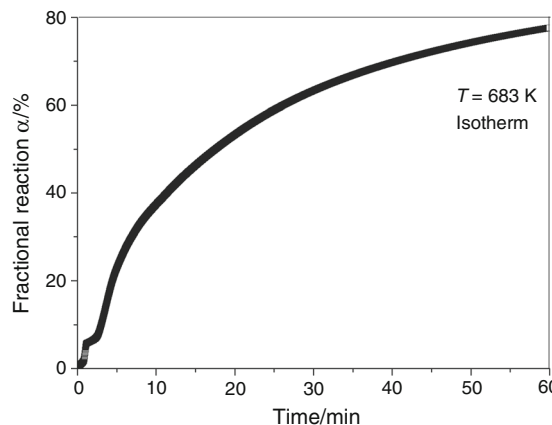


Fig. 8 Isothermal mass-loss trace curves at $T = 683 \text{ K}$ for the thermal decomposition of [AMIM]Cl-PFSA composite membrane

Master plots based on the differential form of the generalized kinetic equation

Using the experimental data of the isothermal mass-loss trace for the thermal decomposition of 10%[AMIM]Cl-PFSA composite membrane under nitrogen atmosphere, the practical usefulness of the master plots was examined. Figure 8 shows the kinetic curves for the thermal decomposition of composite membrane obtained from isothermal mass-loss measurements in 683 K. Using a reference point at $\alpha = 0.5$, Eqs. (9) and (10) can be obtained according to the kinetic analysis of solid-state reactions [44]:

$$\theta = \int_0^t \exp\left(-\frac{E}{RT}\right) dt \tag{9}$$

$$\frac{d\alpha/d\theta}{(d\alpha/d\theta)_{\alpha=0.5}} = \frac{f(\alpha)}{f(0.5)} \tag{10}$$

where θ is generalized time that denotes the reaction time taken to attain a particular α at infinite temperature, $d\alpha/d\theta$ corresponds to the generalized reaction rate, $f(\alpha)$ is differential mechanism function, $f(0.5)$ is a constant for a given kinetic model function. Based on Eq. (11), assuming that the decomposition process follows the first-order reaction kinetics. Figure 9 compares the theoretical master plots of $f(\alpha)/f(0.5)$ against α with the experimental master plots of $(d\alpha/d\theta)/(d\alpha/d\theta)_{\alpha=0.5}$ versus α calculated from the experimental data in Fig. 8. Because the exponential terms in Eq. (11) can be neglected for the isothermal kinetic data, and the experimental master plot for the isothermal kinetic data was obtained as $(d\alpha/d\theta)/(d\alpha/d\theta)_{\alpha=0.5}$ against α . When $\alpha = 0.2-0.5$, it is clearly seen from Fig. 9, the irrespective of the temperature profiles of the kinetic data, the experimental master plots are in good agreement with the theoretical master plot corresponding to the F1 mechanism, its mechanism function $f(\alpha) = (1 - \alpha)$, $g(\alpha) = -\ln(1 - \alpha)$.

$$\frac{d\alpha/d\theta}{(d\alpha/d\theta)_{\alpha=0.5}} = \frac{d\alpha/dt}{(d\alpha/dt)_{\alpha=0.5}} \frac{\exp(E/RT)}{\exp(E/RT_{0.5})} \tag{11}$$

Master plots based on the integral form of the kinetic data

$$\frac{g(\alpha)}{g(0.5)} = \frac{\theta}{\theta_{0.5}} \tag{12}$$

$$g(\alpha) = \int_0^\alpha \frac{d\alpha}{f(\alpha)} = A \int_0^\theta d\theta = A\theta \tag{13}$$

where $g(\alpha)$ is integral mechanism function, because the exponential term in Eq. (13) is a constant during the course

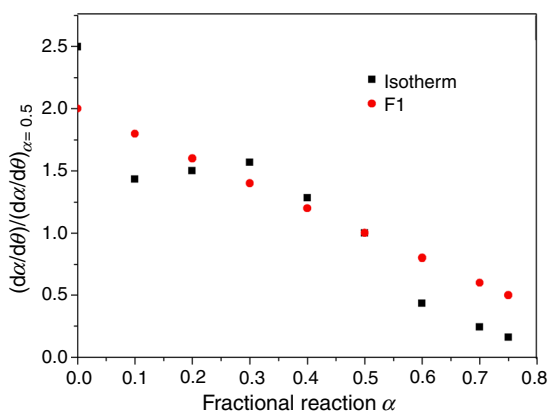


Fig. 9 A comparison of the experimental master plots of $(d\alpha/d\theta)/(d\alpha/d\theta)_{\alpha=0.5}$ against α for the thermal decomposition of [AMIM]Cl-PFSA composite membrane

of the reaction, the value of $\theta/\theta_{0.5}$ at a given α is equivalent to $t/t_{0.5}$. Equation (12) is then transformed into:

$$\frac{g(\alpha)}{g(0.5)} = \frac{t}{t_{0.5}} \tag{14}$$

Based on Eqs. (12) (13) and (14), the experimental master plots of $\theta/\theta_{0.5}$ against α constructed from the experimental isothermal data are shown in Fig. 10. The master plot for the isothermal mass-loss trace was calculated using Eq. (14) as $t/t_{0.5}$ against α . The experimental master plots obtained for the thermal decomposition of [AMIM]Cl/PFSA composite membrane are compared in the same figure with the theoretical master plot corresponding to the F1 kinetic model, its mechanism function $f(\alpha) = (1 - \alpha)$, $g(\alpha) = -\ln(1 - \alpha)$, indicating a close agreement irrespective of quite different temperature programs.

Master plots based on both the integral and differential forms of the kinetic equation

$$\theta \frac{d\alpha}{d\theta} = f(\alpha)g(\alpha) \tag{15}$$

$$\frac{\theta(d\alpha/d\theta)}{\theta_{0.5}(d\alpha/d\theta)_{\alpha=0.5}} = \frac{f(\alpha)g(\alpha)}{f(0.5)g(0.5)} \tag{16}$$

According to Eqs. (15) and (16), the differential-integral master plots, $\theta d\alpha/d\theta$ versus α , are shown in Fig. 11, which were obtained by multiplying the values of $(d\alpha/d\theta)$ and θ at a given α . The experimental master plots for isothermal data fit well the theoretical curve of $f(\alpha) g(\alpha)$ against α corresponding to an F1 kinetic model, but the former curve is slightly shifted to the left.

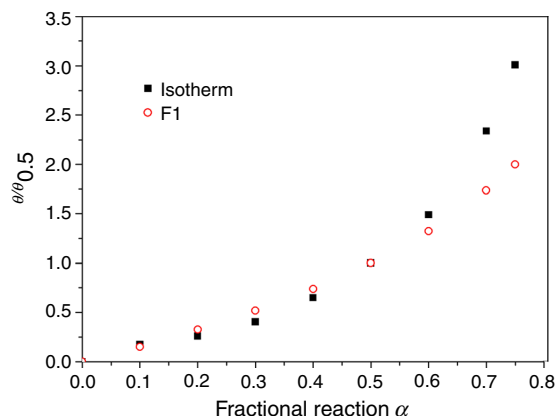


Fig. 10 A comparison of the experimental master plots of $\theta/\theta_{0.5}$ against α for the thermal decomposition of [AMIM]Cl-PFSA composite membrane with the theoretical master curves of $g(\alpha)/g(0.5)$ against α

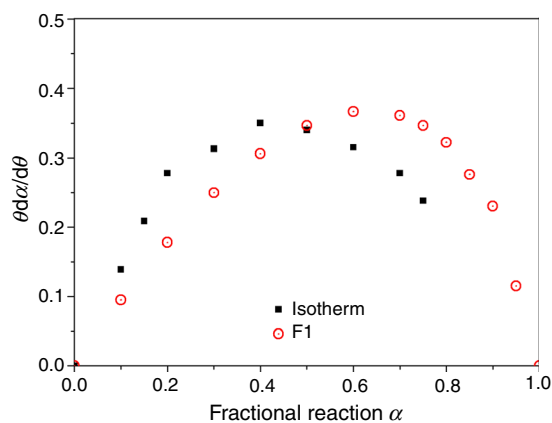


Fig. 11 A comparison of the experimental master plots of $(dx/d\theta)\theta$ against α for the thermal decomposition of [AMIM]Cl-PFSA composite membrane with the theoretical master curves of $f(\alpha)$ $g(\alpha)$ against α

Conclusions

1-Allyl-3-methylimidazolium chloride [AMIM]Cl and triethylamine doped with perfluorinated sulfonic acid composite membranes were prepared. The conductivity of composite membranes was measured. The results showed that when the temperature was raised from 20 to 90 °C, the electrical conductivity of composite membrane is increased from 4.50×10^{-6} to 1.34×10^{-5} S cm^{-1} , compared to un-doping of triethylamine, thermal stability of composite membrane is no significant change, and the [AMIM]Cl-TEA-PFSA exhibits downward trend. However, the peak temperature of [AMIM]Cl-PFSA composite membrane in first stage of thermal degradation almost disappeared owing to the PFSA membrane heat resistant significantly enhanced and offset to high-temperature region. When heated at 350 °C, the conversion rate of PFSA, 10%[AMIM]Cl-PFSA and 10%[AMIM]Cl-TEA-PFSA membrane was 13.71, 3.67 and 1.26% respectively. It can be seen that 10%[AMIM] Cl-TEA-PFSA composite membrane is stable at 350 °C. If the decomposition process follows isothermal first-order reaction and the conversion rate α is 10%, the activation energy E_α of the composite membrane is 97.4 kJ mol^{-1} . In addition, according to the first-order reaction, compared the theoretical master curve with the experimental master plots of the $dx/d\theta/(dx/d\theta)_{\alpha=0.5}$ versus α , the $\theta/\theta_{0.5}$ versus α and the $(dx/d\theta)\theta$ versus α , curve overlap is better, using the isothermal data of 10%[AMIM]Cl-PFSA composite membrane at 683 K.

Acknowledgements This research was financially supported by the following grants: (1) Anhui Province University Students Innovation and Entrepreneurship Program (AH201410361217), (2) Anhui International Science and Technology Cooperation Program (06088018), (3) Huainan Municipal Science and Technology Program (2011A07923). 2016 undergraduate students, Li Yajie, Yang Jie, Zhang Xian and Liu Jinli participated in part of the experimental work.

References

- Liu LY, Chen WD, Li YQ. An overview of the proton conductivity of nafion membranes through a statistical analysis. *J Membr Sci.* 2016;504:1–9.
- Lu YH, Wei F, Lu YW, Liu WL, Li HX, Chen MQ. Effect of pretreated nano-silica on the thermal stability of proton exchange membrane. *Polymer Mater Sci Eng.* 2013;29(1):79–83.
- Matos BR, Arico EM, Linardi M, Ferlauto AS, Santiago EI, Fonseca FC. Thermal properties of Nafion–TiO₂ composite electrolytes for PEM fuel cell. *J Therm Anal Calorim.* 2009;97:591–4.
- Lu YH, Wei F, Lu YW, Ma SH, Li HX, Chen MQ. Effect of tungstophosphoric acid surface treatment on the thermal stability of proton exchange membrane for fuel cell. *Polymer Mater Sci Eng.* 2014;30(5):67–71.
- Subianto S, Mistry MK, Choudhury NR, Dutta NK, Knott R. Composite polymer electrolyte containing ionic liquid and functionalized polyhedral oligomeric silsesquioxanes for anhydrous PEM applications. *Appl Mater interf.* 2009;1(6):1173–82.
- Eguizábal A, Lemus J, Pina MP. On the incorporation of protic ionic liquids imbibed in large pore zeolites to polybenzimidazole membranes for high temperature proton exchange membrane fuel cells. *J Power Sour.* 2013;222:483–92.
- Eren B, Aydin R, Eren E. Morphology and thermal characterization of montmorillonite/polybenzimidazole Nanocomposite. *J Therm Anal Calorim.* 2014;115:1525–31.
- Petreanu I, Ebrasu D, Sisu C, Varlam M. Thermal analysis of sulfonated polymers tested as polymer electrolyte membrane for PEM fuel cells. *J Therm Anal Calorim.* 2012;110:335–9.
- Lee SY, Yasuda T, Watanabe M. Fabrication of protic ionic liquid/sulfonated polyimide composite membranes for non-humidified fuel cells. *J Power Sources.* 2010;195(18):5909–14.
- Bao XJ, Zhang F, Liu QT. Sulfonated poly(2,5-benzimidazole) (ABPBI)/MMT/ionic liquids composite membranes for high temperature PEM applications. *Int J Hydrogen Energy.* 2015;40:16767–74.
- Ye H, Huang J, Xua JJ. New membranes based on ionic liquids for PEM fuel cells at elevated temperatures. *J Power Sources.* 2008;178(2):651–60.
- Wang JTW, Hsu SLC. Enhanced high-temperature polymer electrolyte membrane for fuel cells based on polybenzimidazole and ionic liquids. *Electrochim Acta.* 2011;56(7):2842–6.
- Blanco I, Cicala G, Latteri A, Mamo A, Recca A. Thermal and thermo-oxidative degradations of poly(2,6-dimethyl-1,4-phenylene oxide) (PPO)/copoly(aryl ether sulfone)P(ESES-co-EES) block copolymers: a kinetic study. *J Therm Anal Calorim.* 2013;112:375–81.
- Yi SZ, Zhang FF, Li W. Anhydrous elevated temperature polymer electrolyte membranes based on ionic liquids. *J Membr Sci.* 2011;366(1/2):349–55.
- Che QT, He RH, Yang JS. Phosphoric acid doped high temperature proton exchange membranes based on sulfonated polyether ether ketone incorporated with ionic liquids. *Electrochem Commun.* 2010;12(5):647–9.
- Monda AN, Tripathi BP, Sbahi VK. Highly stable apmtic ionic-liquid doped anhydrous proton-conducting polymer electrolyte membrane for high temperature applications. *J Mater Chem.* 2011;21(12):4117–24.
- Ye H, Huang J, Xu JJ, Kodiweera NKAC, Jayakody JRP, Greenbaum SG. New membranes based on ionic liquids for PEM fuel cells at elevated temperatures. *J Power Sources.* 2008;178:651–60.
- Shaplov AS, Vlasov PS, Lozinskaya EI, Ponkratov DO, Malyskhina IA, Vidal F, Okatova OV, Pavlov GM, Wandrey C, Bhide A, Schonhoff M, Vygodskii YS. Polymeric ionic liquids: comparison of polycations and polyanions. *Macromolecules.* 2011;44:9792–803.

19. Rao CJ, Krishnan RV, Venkatesan KA, Nagarajan K, Srinivasan TG. Thermochemical properties of some bis(trifluoromethylsulfonyl) imide based room temperature ionic liquids. *J Therm Anal Calorim.* 2009;97:937–43.
20. Lebga-Nebane JL, Rock SE, Franclemont J, Roy D, Krishnan S. Thermophysical properties and proton transport mechanisms of trialkylammonium and 1-alkyl-1H-imidazol-3-ium protic ionic liquids. *Ind Eng Chem Res.* 2012;51:14084–98.
21. Yu L, Pizio BS, Vaden TD. Conductivity and spectroscopic investigation of bis(trifluoromethanesulfonyl) imide solution in ionic liquid 1-butyl-3-methylimidazolium bis(trifluoromethanesulfonyl)imide. *J Phys Chem B.* 2012;116:6553–60.
22. Díaz M, Ortiz A, Ortiz I. Progress in the use of ionic liquids as electrolyte membranes in fuel cells. *J Membr Sci.* 2014;469:379–96.
23. Bentley CL, Bond AM, Hollenkamp AF, Mahon PJ, Zhang J. Mass transport studies and hydrogen evolution at a Platinum electrode using bis(trifluoromethanesulfonyl) imide as the proton source in ionic liquids and conventional solvents. *J Phys Chem C.* 2014;118:29663–73.
24. Sambasivarao SV. Thermal stability and ionic conductivity of high-temperature proton conducting ionic liquid–polymer composite electrolyte membranes for fuel cell applications, *Polymer Composites for Energy Harvesting, Conversion, and Storage.* ACS Symposium Series; American Chemical Society: Washington DC (2014).
25. Sood R, Iojoiu C, Espuche E, Gouanvé F, Mendil-Jakani H, Lyonard S. Influence of different perfluorinated anion based ionic liquids on the intrinsic properties of Nafions. *J Membr Sci.* 2015;495:445–56.
26. Lemus J, Eguizabal A, Pina MP. UV polymerization of room temperature ionic liquids for high temperature PEMs: study of ionic moieties and crosslinking effects. *Int J Hydrogen Energy.* 2015;40:5416–24.
27. Perdikaki AV, Labropoulos AI, Siranidi E, Karatasios I, Kanellopoulos N, Boukos N, Falaras P, Karanikolos GN, Romanos GE. Efficient CO oxidation in an ionic liquid-modified, Au nanoparticle loaded membrane contactor. *Chem Eng J.* 2015;305:79–91.
28. Salar-García MJ, Ortiz-Martínez VM, Ríos AP, Hernández-Fernández FJ. A method based on impedance spectroscopy for predicting the behavior of novel ionic liquid-polymer inclusion membranes in microbial fuel cells. *Energy.* 2015;89:648–54.
29. Akbar MM, Chemat F, Arunagiri A, Murugesan T. Density and excess properties of N-methyldiethanolamine (MDEA) with 1-hexyl-3-methylimidazolium tris(pentafluoroethyl) trifluorophosphate [hmim][FAP]. *J Therm Anal Calorim.* 2016;123:785–91.
30. Angell CA, Byrne N, Belieres JP. Parallel developments in aprotic and protic ionic liquids: physical chemistry and applications. *Acc Chem Res.* 2007;40(11):1228–36.
31. Padilha JC, Basso J, Trindade LG, Martini EMA, Souza MO, Souza RF. Ionic liquids in proton exchange membrane fuel cells: efficient systems for energy generation. *J Power Sources.* 2010;195:6483–5.
32. Martinez M, Molmeret Y, Cointeaux L, Iojoiu C, Lepretre JC, Kissi NE, Judeinstein P, Sanchez JV. Proton-conducting ionic liquid-based Proton Exchange Membrane Fuel Cell membranes: the key role of ionomer–ionic liquid interaction. *J Power Sources.* 2010;195:5829–39.
33. Feng WQ, Lu YH, Chen Y, Lu YW, Yang T. Thermal stability of imidazolium-based ionic liquids investigated by TG and FTIR techniques. *J Therm Anal Calorim.* 2016;125:143–54.
34. Ye YS, Tseng CY, Shen CY. A new graphene- modified protic ionic liquid-based composite membrane for solid polymer electrolytes. *J Mater Chem.* 2011;21(28):10448–53.
35. Langevin D, Nguyen QT, Marais S, Karademir S, Sanchez JY, Iojoiu C, Martinez M, Mercier R, Judeinstein P, Chappey C. High-temperature ionic-conducting material: advanced structure and improved performance. *J Phys Chem C.* 2013;117:15552–61.
36. Maity S, Singha S, Jana T. Low acid leaching PEM for fuel cell based on polybenzimidazole nanocomposites with protic ionic liquid modified silica. *Polymer.* 2015;66:76–85.
37. Diaz M, Ortiz A, Vilas M, Tojo E, Ortiz I. Performance of PEMFC with new polyvinyl-ionic liquids based membranes as electrolytes. *Int J Hydrogen Energy.* 2014;39:3970–7.
38. Malik RS, Tripathi SN, Gupta D, Choudhary V. Novel anhydrous composite membranes based on sulfonated poly (ether ketone) and aprotic ionic liquids for high temperature polymer electrolyte membranes for fuel cell applications. *Int J Hydrogen Energy.* 2014;39:12826–34.
39. Yooa S, Won J, Kang SW, Kang YS, Nagase S. CO₂ separation membranes using ionic liquids in a Nafion matrix. *J Membr Sci.* 2010;363:72–9.
40. Neves LA, Benavente J, Coelho IM, Crespo JG. Design and characterization of Nafion membranes with incorporated ionic liquids cations. *J Membr Sci.* 2010;347:42–52.
41. Lu L, Huang XR, Qu YB. Effect of the structure of imidazolium cations in [BF₄][−] type ionic liquids on direct electrochemistry and electrocatalysis of horseradish peroxidase in Nafion films. *Colloids Surf B.* 2011;87:61–6.
42. Yang JS, Che QT, Zhou L. Studies of a high temperature proton exchange membrane based on incorporating an ionic liquid cation 1-butyl-3-methylimidazolium into a Nafion matrix. *Electrochim Acta.* 2011;56(17):5940–6.
43. Vyazovkin S, Burnham AK, Criado JM, Pérez-Maqueda LA, Popescu C, Sbirrazzuoli N. ICTAC Kinetics Committee recommendations for performing kinetic computations on thermal analysis data. *Thermochim Acta.* 2011;520:1–19.
44. Gotor FJ, Criado JM, Malek J, Koga N. Kinetic analysis of solid-state reactions: the Universality of master plots for analysing isothermal and non-isothermal experiments. *J Phys Chem A.* 2000;104:10777–82.